Optimized LQR Control for Dual-Input Boost Converter in Hybrid PV-Wind System for Remote Telephony Applications

Aruna RAJENDRAN[1]*, Raja JAYAMANI[2], Moorthi KIRUBAN[3]

[1,2] Department of Electronics and Communication Engineering, Adhiparasakthi Engineering College, Melmaruvathur, Kancheepuram, 603319, Tamil Nadu, India
arrrunarajendran@gmail.com (**Corresponding author*), raja@apec.edu.in

[3]Department of Electronics and Communication Engineering, Sri Sairam Engineering College, Sai Leo Nagar, West Tambaram, Chennai, 600132, Tamil Nadu, India
moorthi.ece@sairam.edu.in

Abstract: This paper proposes an optimized Linear Quadratic Regulator (LQR) based control scheme for a modified Cuk-SEPIC dual-input DC-DC converter fed by hybrid photovoltaic (PV) and wind energy sources, specifically designed for supplying regulated DC power to off-grid telecommunication loads in remote areas. The converter topology combines the advantages of the Cuk and SEPIC structures, ensuring a continuous input current, a wide operating range, and an improved voltage gain, which makes it ideal for PV-wind systems experiencing variable input conditions. A dynamic state-space model of this hybrid system is developed, incorporating system states such as the inductor current and the output voltage. The LQR controller is synthesized for minimizing a quadratic cost function that penalizes both the output voltage deviations and the excessive control effort. The optimal selection of the state and input weighting matrices enables a robust response under varying solar irradiance and wind speed conditions and load disturbances. The simulation results demonstrate that the proposed LQR-controlled system achieves a fast voltage regulation, with a minimal overshoot and a strong resilience against input and load variations, which makes it suitable for powering remote, off-grid telecommunication base stations and communication nodes where power reliability is critical.

Keywords: Hybrid solar-wind sources, Modified Cuk-SEPIC converter, Linear Quadratic Regulator, MATLAB/Simulink.

1. Introduction

The growing energy crisis and the increasing demand for fossil fuels have directed public attention towards sustainable power generation from green energy sources. Among these, the hybridization of solar and wind energy systems has gained significant attention due to its complementary nature and enhanced reliability. However, the intermittent availability of these resources necessitates the inclusion of supplemental energy storage systems (batteries and fuel cells) in order to ensure a continuous power supply (Ssenyimba, Kiggundu & Banadda, 2020; Icaza et al., 2020; Eltamaly et al., 2021). The case studies of Al-Ghussain et al. (2023) and Yao et al. (2020) have emphasized the critical role of renewable energy adoption in addressing global energy challenges. These studies demonstrated the feasibility and economic viability of hybrid systems combining solar PV and wind power generation. Such integrated systems not only optimize energy production, but they also reduces the carbon footprint, which makes them a promising solution for sustainable energy development. However, to ensure the seamless integration of hybrid systems, converters plays a vital role and they enable the practical use of RES by addressing the challenges posed by environmental variability.

Numerous converter topologies have been formulated to facilitate the integration of multiple Renewable Energy Sources (RES), particularly Multi-Input Single-Output (MISO) (Soldado-Guamán et al., 2023), and Single/Dual Input Dual-Output converters. These multiport converter architectures offer significant flexibility in managing energy from diverse sources such as solar PV, wind, and fuel cells. However, these systems often feature a reduced efficiency due to increased conduction and switching losses, especially under varying environmental and load conditions.

In HRES configurations, RES like solar and wind are often connected in parallel through a multiport DC converter to manage energy flow and reduce source intermittency. These converters enhance system flexibility and efficiency by enabling the simultaneous power transfer and dynamic load management. To handle the system's nonlinear nature, Lyapunov-based control strategies are applied, offering a robust stability and an improved disturbance rejection. However, these systems face certain drawbacks such as a complex control design, a high computational load and sensitivity to model inaccuracies (Mechnane et al., 2023). The integration of RES using an extendable multiport DC boost converter has been analysed.

https://doi.org/10.24846/v34i4y202505

An ANFIS controller was incorporated to regulate the converter's output voltage, offering intelligent control under varying source conditions. However, this approach involves a high system complexity due to the presence of multiple sources and advanced control algorithms. The reliance on accurate real-time data and an increased component count can affect cost and scalability (Paul, Kumar & Carol, 2021). Several studies have proposed advanced MISO models for integrating RES into grid or microgrid applications (Ravada, Tummuru & Ande, 2020; Jha et al., 2022; Cholamuthu et al., 2022). However, such approaches often involve complex modeling, high computational requirements and dependence on precise real-time data. To overcome this problem, modifications in the SEPIC converter has been developed (Jyothi et al., 2023; Mandal & Prabhakaran, 2023). Okilly & Baek (2021) investigated power factor correction (PFC) topologies suited for high-power telecom applications. Two boost converter designs, a conventional PFC and a bridge interleaved CCM PFC are evaluated through detailed modeling, optimal control design, and hardware implementation. But the limitations of traditional converters (SEPIC and Cuk) in achieving a high voltage gain and efficiency have led researchers to shift toward hybrid converters (Nirmala & Venmathi, 2024).

Therefore, a high-gain, low-loss converter was designed to support the integration of RES into the grid by matching voltage levels effectively. The proposed topology combines a boost converter with a voltage multiplier (VM) cell and a switched capacitor network to achieve an elevated voltage gain. However, the complexity of VM cells and switched capacitor networks may affect scalability (Sathiya & Arun Noyal Doss, 2023). Among the hybrid converters, the Cuk-SEPIC converter is preferred due to its ability to perform both step-up and step-down operations with continuous input and output currents, reducing the ripple and improving efficiency. It offers a higher voltage gain, lower component stress and better power quality in comparison with standalone converters.

A novel single-phase Cuk-SEPIC PFC converter was designed to operate in Discontinuous Conduction Mode (DCM) under varying load and input conditions. While its performance is promising, the operation in DCM may limit its efficiency at higher loads and require a precise timing control (Shunmathi & Gnanavadivel, 2024). Further on, a single-stage bridgeless (BL) Cuk-SEPIC converter for electric vehicles (EVs) with battery charging was proposed in (Kushwaha, Singh & Khadkikar, 2021).

The design of Cuk and SEPIC converter topologies for PV applications, particularly in the context of achieving high-voltage conversion ratios was formulated in (Tenali, Ansari & Praveen, 2021).

Despite their advantages, the Cuk-SEPIC converters face limitations such as a reduced efficiency in DCM at higher loads, increased switching losses and control complexity (Khan et al., 2023; Shen et al., 2023; Saha et al., 2025). Thus, this paper proposed a modified Cuk–SEPIC converter for achieving an optimized power conversion with a reduced loss.

Controllers are required to regulate and stabilize the output voltage and current efficiently under varying input conditions. To improve the converter performance, various control techniques are employed (Duraisamy, 2024; Salimi, Radmand & Firouz, 2021). A Boost converter with PID control (Mamat & Ishak, 2022) and an optimized PI controller (Vijayakumar & Sudhakar, 2024; Katche et al., 2023) have been incorporated. However, the PI controller lacks the ability to handle multivariable systems and optimize their performance based on a cost function. Hence, this work introduced the LQR controller which offers an optimal, state-based control with an improved dynamic response and system stability.

Thus, the key performance of the proposed controller includes:

- The precise regulation of the DC output voltage under varying solar and wind input conditions, an enhanced dynamic response with a reduced overshoot and settling time, and an optimal power sharing between PV and wind sources;
- Battery management, which includes monitoring the state of charge (SoC), managing the charging and discharging modes, and preventing overcharging;
- Achieving a lower current and voltage ripple, and improving the overall converter efficiency and reducing component stress.

These functions ensure system stability, maximize energy efficiency, and guarantee an uninterrupted

power supply to remote telecom loads under varying environmental conditions. This hybrid configuration of PV and wind energy systems is adopted in this study owing to their complementary power generation profiles and superior overall efficiency. This complementary nature ensures a more uniform and reliable power supply over time in comparison with standalone sources. Moreover, integrating these two renewable sources through the modified Cuk–SEPIC converter enables an efficient energy sharing and minimizes the conversion losses. The converter topology ensures continuous input currents, a reduced voltage ripple, and a high voltage gain, leading to a better utilization of the available renewable energy.

The remainder of this paper is as follows. Section 2 describes the proposed system architecture, the modified Cuk–SEPIC converter operation, and the detailed mathematical modelling used for controller development. Section 3 presents the simulation results that validate the effectiveness of the LQR-controlled converter under varying source conditions. Further on, Section 4 sets forth the hardware implementation and experimental verification of the proposed system, along with a comparative performance analysis. Finally, Section 5 concludes this paper by highlighting the key outcomes and the suitability of the proposed hybrid PV–wind converter for remote telecommunication applications.

2. Topology Description and Modelling

The block diagram of the proposed system is presented in Figure 1. In this diagram, wind and PV sources are accommodated using a single-stage DC-DC converter. It considers the perturbation & observation (P&O) MPPT for the wind and PV sources. The proposed system is able to feed the remote telecommunication load with solar-wind energy sources or an individual PV/wind energy source according to availability. For that, an embedded controller is programmed. The controller is also able to maintain a constant power at the load point. The battery is used as a backup source, for compensating the required load demand.

A MATLAB code is implemented for monitoring the battery voltage, current, and state of charge (SOC) estimation.

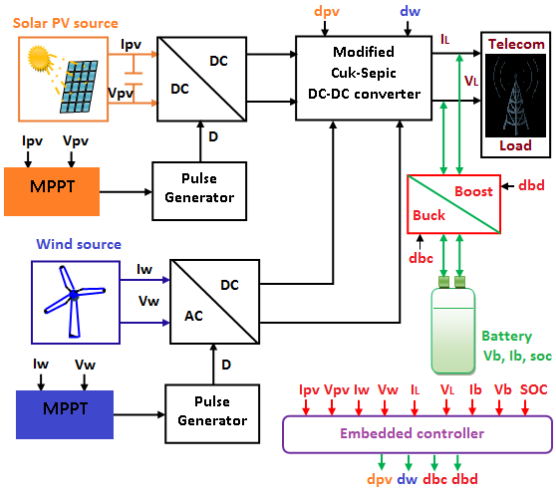

Figure 1. Block diagram of the PV-wind system-based modified Cuk-SEPIC DC-DC converter

2.1 Modified Cuk-SEPIC Converter - Design and Working

The topology of the proposed modified Cuk-SEPIC converter is illustrated in Figure 2.

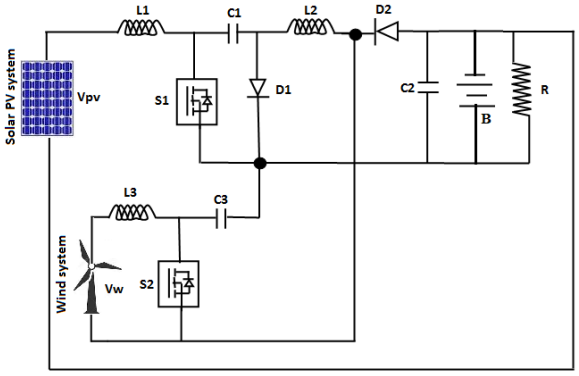

Figure 2. Modified Cuk-SEPIC converter topology

The proposed hybrid converter integrates PV and wind sources using a modified Cuk-SEPIC dual-input DC/DC converter for supplying a regulated DC output to the telecommunication load. The PV source powers the system through an inductor-capacitor network involving the switch S1, while the wind source does so via a SEPIC-based leg controlled by switch S2. Both energy paths share a common inductor and diode for power delivery to the output capacitor and load. The converter operates in a continuous conduction mode, ensuring a smooth energy transfer with minimal ripple. A LQR controller dynamically adjusts the switching duty cycles based on state feedback to maintain a stable output voltage under fluctuating source conditions. This ensures a reliable and efficient

power flow with reduced switching losses. The simulation parameters employed for the solar and wind systems are mentioned in Table 1.

Table 1. Specifications – PV/wind system

Parameter	Values
Solar PV system rating	75 V, 22.5A, 1.5kW
Insolation, Temperature	900 W/m^2, 25^{o}C
Wind power system rating	60V, 23A, 1.4kW
Rated speed of PMSG	1500 rpm
Wind speed	3m/s

On applying the volt-second balance equations the output voltage of a system can be calculated as follows:

$$(d_1 * V_{PV}) + ((1-d_1) * (V_{PV} - V_{C1} - V_{C2})) = 0 \quad (1)$$

$$d_2 (V_{C1} + V_{C3}) + (d_1 - d_2) V_{C3} - (1-d_1) V_{C2} = 0 \quad (2)$$

$$d_2 (V_W - V_{C2}) + (1-d_2)(V_W - V_{C3} - V_{C2}) = 0 \quad (3)$$

Based on equations (1), (2) and (3), equation (4) is obtained:

$$V_O = V_{C2} = (1-d_2)\frac{d_1}{(1-d_1)} V_{PV} + d_2 V_W \quad (4)$$

where the Solar PV voltage and wind voltage are denoted by V_{PV} (V1) and V_W (V2), whereas the corresponding duty cycles are denoted by d_1 and d_2. Equation (4) gives the output voltage.

The circuit diagrams equivalent to the system's four modes of operation are shown in Figure 3(a–d) and the working principles are rendered in Table 2.

On applying Kirchhoff's Voltage Law (KVL) and Kirchhoff's Current Law (KCL) to the proposed converter, the averaged state equations (equation (5) to equation (11)) are given as follows:

$$[\dot{X}] = [\bar{A}]\, x + [\bar{B}]\, u \quad (5)$$

$$\frac{di_{L1}}{dt} = -\frac{1}{L1} * (1-d_1) * V_{C1} + \frac{1}{L1} * (V_{C2} + V1) \quad (6)$$

$$\frac{di_{L2}}{dt} = \frac{1}{L2} * d_2 * V_{C1} - \frac{1}{L2} * (1-d_2) V_{C2} + \frac{d_2}{L2} * V_{C3} \quad (7)$$

$$\frac{di_{L3}}{dt} = -\frac{1}{L3} * (1-d_2-d_1d_2) * V_{C3} - \frac{1}{L3} * (1-d_2) V_{C2} + \frac{1}{L3} * V2 \quad (8)$$

$$\frac{dV_{C1}}{dt} = \frac{1}{C1} * (d_2) * i_{L1} + \frac{1}{C1} * (1-d_2) * i_{L2} \quad (9)$$

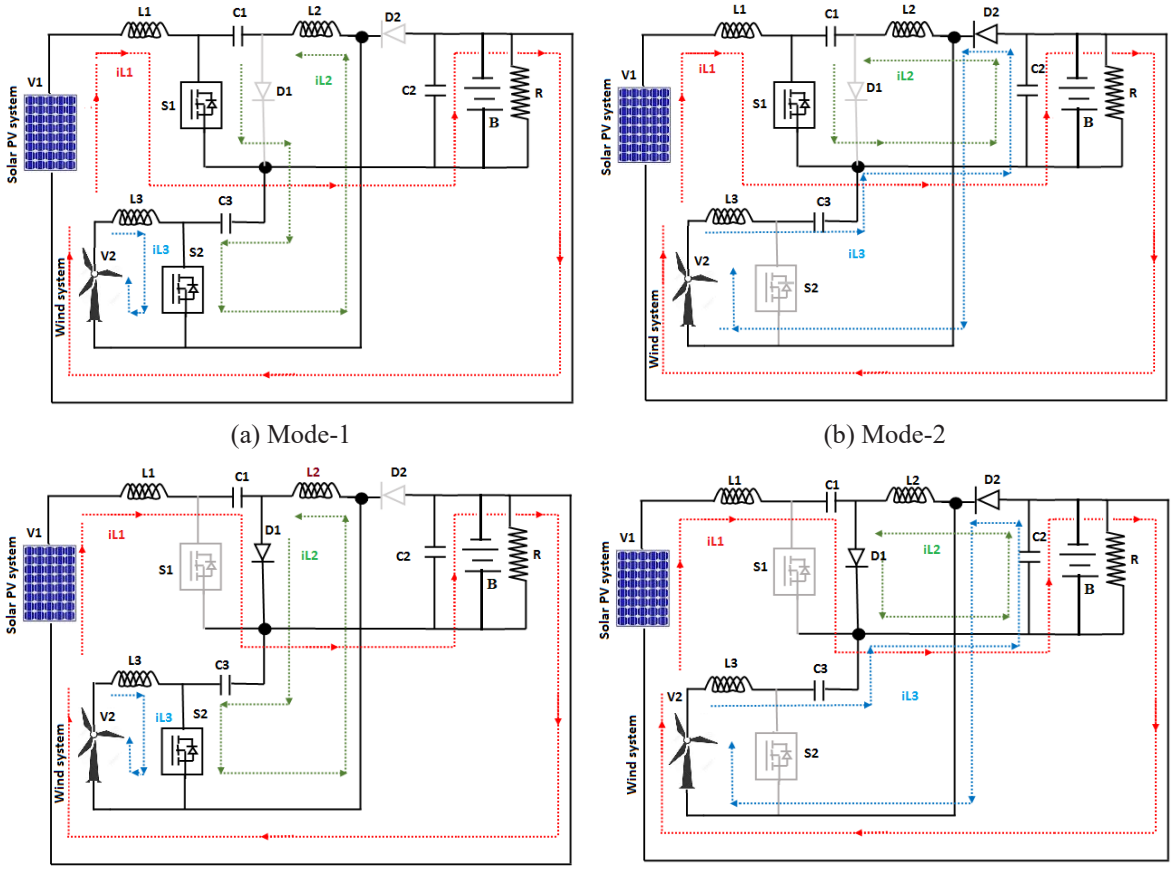

(a) Mode-1

(b) Mode-2

(c) Mode-3

(d) Mode-4

Figure 3. Operating Modes

$$\frac{dV_{C2}}{dt} = \frac{1}{C2} * i_{L2} + \frac{1}{(R*C2)} * V_{C2} \quad (10)$$

$$\frac{dV_{C3}}{dt} = \frac{1}{C3} * (1-d_1) * (1-d_2) * i_{L1} + \frac{1}{C3} * (1-d_2) * i_{L2} + \frac{1}{C3} * i_{L3} \quad (11)$$

In equations (5)–(11), x represents the state vector of inductor currents and capacitor voltages, while u denotes the control input consisting of the duty cycles. The matrices A and B define the system's linearized dynamics, and parameters L,C,R correspond to the converter's inductances, capacitances, and load resistance.

Table 2. Modes of operation

Mode	S1	S2	Working
1	ON	ON	D1, D2 are in reverse biased. The solar power source charges the inductor L1 and feeds the load, while L3 is charged by the wind source. The stored energy of C1 and C3 is delivered to L2.
2	ON	OFF	D1 is in reverse bias, D2 is in forward bias. The inductor L1 and the load are charged by the solar power source. The Wind power source and the energy stored in L3 feed the load and charge the capacitor C3. The energy in capacitor C1 feeds the load and inductor L2.
3	OFF	ON	D1 is in forward bias and D2 is in reverse bias. The wind power source charges the inductor L3. The solar power source and the energy stored in inductor L1 feeds the load and charges the capacitor C1. The energy in capacitor C3 charges the inductor L2.
4	OFF	OFF	D1 and D2 are in forward bias. The solar power source and the energy stored in L1 charge the capacitor C1 and feed the load. The wind power source and the energy stored in L3 charge the capacitor C3 and the load. The energy stored in L2 feeds the load.

2.2 LQR Controller Design

The LQR controller design is based on the optimal control theory, which aims to determine the control input (u(t)) that minimizes a predefined quadratic cost function. For the proposed converter system with PV and wind sources as input, the cost function is expressed as:

$$J = \int_0^{\infty} \left(x^T Q x + u^T R u \right) dt \quad (12)$$

where (x) is the state vector comprising converter inductor currents and output voltage, and (u) denotes the control inputs corresponding to the duty cycles of switches.

The weighting matrices (Q) and (R) are selected to penalize the deviations in key system characteristics and excessive control effort, respectively. The optimal control law is then derived as:

$$u(t) = -Kx(t) \quad (13)$$

where (K) is the optimal feedback gain matrix.

This theoretical formulation ensures that the converter output voltage remains regulated and stable under varying PV and wind input conditions while minimizing the switching effort. The controller's optimal feedback structure enhances the system stability, reduces the overshoot and settling time and achieves an efficient power sharing between the two renewable sources. These theoretical foundations are further validated through simulation and hardware results demonstrating an improved transient and steady-state performance.

2.3 State Space Model

To derive the state space model, small signal variables should be added with the averaged equations. This is done by representing each variable as a combination of a DC and AC value. Linearization leads to the following small signal equations (equations (14) to (20)), in which the hat denotes the perturbation from the steady state working points (X, U):

$$\hat{X} = A\hat{x} + B\hat{u} + E\hat{d} \quad (14)$$

$$\frac{d\widehat{i_{L1}}}{dt} = \frac{1}{L1} * \left(-V_{C1}(1-D1) + V_1 + V_{C2} \right) + \frac{1}{L_1} * \left(-\widehat{V_{C1}}(1-D1) + \hat{d_1} * V_{C1} + \widehat{V_{C2}} + \widehat{V1} \right) \quad (15)$$

$$\frac{d\widehat{i_{L2}}}{dt} = \frac{1}{L2} * \left(D2 * V_{c1} - V_{c2}(1-D2) + D2 * V_{C3} \right) + \frac{1}{L_2} * \begin{pmatrix} D_2 * \widehat{v_{C1}} \\ + \hat{d_2} * V_{C1} - \widehat{v_{C2}}(1-D2) + D2 * \widehat{v_{C3}} \\ + \hat{d_2} * (V_{C2} + V_{C3}) \end{pmatrix} \quad (16)$$

$$\frac{d\widehat{i_{L3}}}{dt} = \frac{1}{L3} * \left(V2 - V_{C2}(1-D2-D1D2) - V_{C3}(1-D2) \right) + \frac{1}{L3} * \begin{pmatrix} -(1-D2-D1D2) * \widehat{v_{C2}} + \\ \hat{d_2} * (V_{C2} + V_{C3}) + \\ \widehat{v_2} - \widehat{V_{C3}} * (1-D2) \end{pmatrix} \quad (17)$$

$$\frac{d\widehat{V_{C1}}}{dt} = \frac{1}{C1} * \left[D2 * I_{L1} + (1-D2) * I_{L2} \right] + \frac{1}{C1} * \left[D2 * \widehat{i_{L1}} - \widehat{(1-d_2)} * (I_{L2} - I_{L1}) + (1-D2) * \widehat{I_{L2}} \right] \quad (18)$$

$$\frac{d\widehat{V_{C2}}}{dt} = \frac{1}{R*C2} * \left(V_{C2} + R * I_{L2} \right) + \frac{1}{R*C2} * \left(R * \widehat{i_{L2}} + \widehat{v_{C2}} \right) \quad (19)$$

$$\frac{d\widehat{V_{C3}}}{dt} = \frac{1}{C3} \left[I_{L3} + (1-D2) I_{L2} + (1-D1)(1-D2)(I_{L1}) \right] + \frac{1}{C3} * \left[\widehat{i_{L3}} - \widehat{(1-d_2)} * (I_{L2}) + (1-D_2) * \widehat{i_{L2}} \right] + \widehat{(1-d_1)} \quad (20)$$

Then perturbation and Laplace transform equation is written by using equation (21):

$$\frac{\widehat{X(s)}}{\widehat{U(S)}} = (SI - A)^{-1} * (E * F(S)) \quad (21)$$

Equation (21) expresses the small-signal state response in the Laplace domain, where X(s) and U(S) represent perturbations around steady-state values. The term $(SI-A)^{-1}$ acts as the resolvent matrix, defining how system dynamics shapes these perturbations. The matrix E couples the external disturbances denoted by F(S) to the state, enabling a complete linearized representation of the small-signal behavior.

$$A = \begin{bmatrix} 0 & 0 & 0 & \frac{1}{L1}(1-D1) & \frac{1}{L1} & 0 \\ 0 & 0 & 0 & \frac{1}{L2}(D2) & \frac{1}{L2}(1-D2) & \frac{1}{L2}(D2) \\ 0 & 0 & 0 & 0 & \frac{1}{L3}\begin{bmatrix}1-D2 \\ -D1D2\end{bmatrix} & \frac{1}{L3}(1-D2) \\ \frac{1}{C2}(D2) & \frac{1}{C2}(1-D2) & 0 & 0 & 0 & 0 \\ 0 & \frac{1}{C2} & 0 & 0 & \frac{1}{R*C2} & 0 \\ \frac{1}{C3}\begin{bmatrix}(1-D1) \\ (1-D2)\end{bmatrix} & \frac{1}{C3}(1-D2) & \frac{1}{C3} & 0 & 0 & 0 \end{bmatrix}$$

$$B = \begin{bmatrix} \frac{1}{L_1} \\ 0 \\ \frac{1}{L_3} \\ 0 \\ 0 \\ 0 \end{bmatrix} \text{ and } E = \begin{bmatrix} 0 & 0 & 0 & 0 & \frac{V_{C1}}{L1} & 0 \\ 0 & 0 & 0 & 0 & 0 & \frac{1}{L2}(D2) \\ 0 & 0 & 0 & 0 & 0 & \frac{1}{L3}(1-D2) \\ 0 & 0 & 0 & 0 & \frac{I_{L2}-I_{L1}}{C1} & 0 \\ 0 & 0 & 0 & 0 & 0 & 0 \\ 0 & 0 & 0 & 0 & 0 & 0 \end{bmatrix} \quad (22)$$

The transfer function linking the ouput capacitor voltage (Vc_2) to the duty cycle (d_2) is as follows:

$$\frac{\widehat{V_{C2}}}{\hat{d}_2} = \frac{\begin{array}{l}(S^4(L2L3C2C3D2R)(L1L3C3C2D2R)+(L1L3C1C3D2R)) \\ +\left((L3)*(I_{L2}-I_{L3})*\left(\begin{array}{l}(L1L2C1)+ \\ (D2L1C1C2R)S^3\end{array}\right)\right)-(C1L1D2RS^2)\end{array}}{\begin{array}{l}(L1L2L3C1C2C3RS^5)-(L1L2L3C1C3S^5)+S^4\left(\begin{array}{l}((L1L3C1C2D2R)+(L1L3C1C3D2R)+ \\ (L1L3C2C3D2R)+(L2L3C2C3D2R))\end{array}\right)+ \\ (S^3((L1L3C1D2)+(L1L3C3D2)+(L1L2C1D2))) \\ +((S^2(L1C1D2R)+(L1C2D2R)+(L2C2D2R))) \\ +(S((L3D2)+(L1D2)+(L2D2)))+((C1D2R))\end{array}} \quad (23)$$

where A is the system matrix, B is the input matrix and E represents the disturbance.

Once the state-space model of the converter is derived, the next step is to design the LQR controller. The goal is to regulate the output voltage and ensure an optimal power sharing between the PV and wind sources. First the appropriate weighting matrices Q and R are chosen. Q penalizes deviations in key states characteristics (like output voltage), while R penalizes excessive control effort (duty cycle changes). Using these matrices, the optimal gain matrix K is computed by solving the Riccati equation, typically with the MATLAB's LQR function (A, B, Q, R). This results in equation (13), where the control input u(t) (duty cycles) depends on the measured states x(t). The computed duty cycles are then applied for controlling the converter switches. This ensures that the system maintains a stable DC output even under changing solar power, wind power and load conditions. The LQR controller thus enables a fast, efficient, and reliable performance for remote telephony power systems.

3. Simulation Results and Discussions

When accommodating the controller block in the modified Cuk-SEPIC topology, it is desired to maintain a constant power, which is achieved by using the novel embedded controller. The Cuk-SEPIC and Modified Cuk-SEPIC topologies are simulated using a mathematical software package called MATLAB with the parameters given in Table 3.

Table 3. Simulation Configuration

Parameters		Modified Cuk-SEPIC
Inductors (Henry)	L1 L2 L3	158e-6 89.16e-6 158e-6
Capacitors (Farad)	C1 C2 C3	2906e-6 1132.42e-6 1132.42e-6
Load	DC	1.2 kW
Frequency	F	20 KHz
Battery	Storage	48V,200 Ah
Input	V1	65V, 23A
Input	V2	55V, 25A

Figure 4 illustrates the converter's output voltage and current under controlled and uncontrolled conditions.

In the first case (without controller), the output voltage gradually decreases to about –60 V, while the current is reduced to –30 A within 1 second, indicating a slower dynamic response. In the second case, both the voltage and current exhibit a lower settling time around 0.06 sec and reach the steady values of nearly –50 V and –25 A respectively, showing a faster stabilization. This comparison highlights that the system attains a stable operation in both scenarios, but the second case reveals an improved damping and quicker transient settling time in comparison with the first one.

Figures 5 and 6 present the voltage and current characteristics for the inductors and capacitors, respectively.

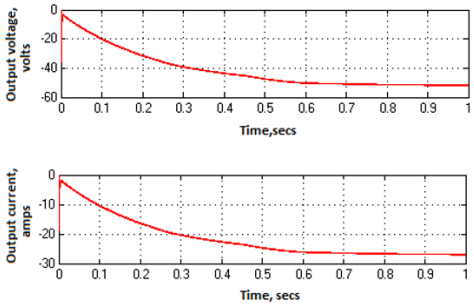

(a) Output voltage and current when the controller is not employed

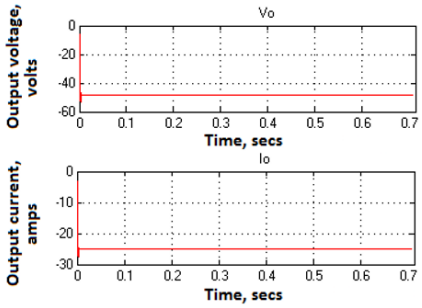

(b) Output voltage and current when the controller is employed

Figure 4. Output voltage & current

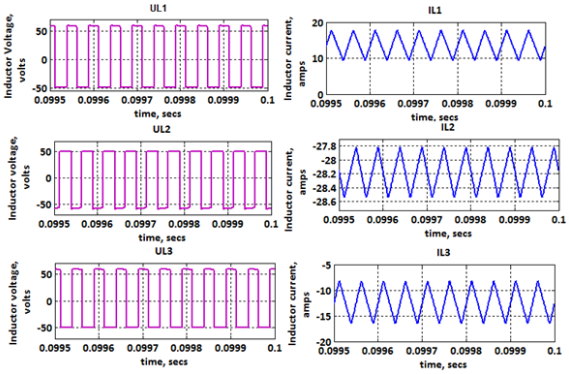

Figure 5. Voltage and current through the Inductors

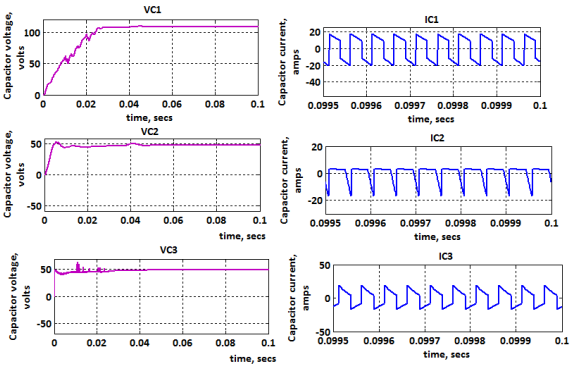

Figure 6. Voltage and current through the Capacitors

From this analysis, it is evident that the proposed modified Cuk-SEPIC converter achieves a faster stabilization in comparison with conventional configurations. The results further confirm its reliability and stability, ensuring a consistent operational performance. Therefore, the proposed system proves capable of efficiently managing different combinations of input power sources to satisfy the load demand with the support of the controller outputs.

4. Hardware Results

As shown in Figure 7, a prototype model for the efficient modified Cuk-SEPIC converter topology was implemented with the parameters L1 with the value of 158µH, L2 with the value of 84.19µH, C1 with the value of 2904.5µF, C2 with the value of 1132.42µF, R with the value of 25 Ω, and 420 watts, V1 with the value of 60V, V2 with the value of 60V and the switching frequency with the value

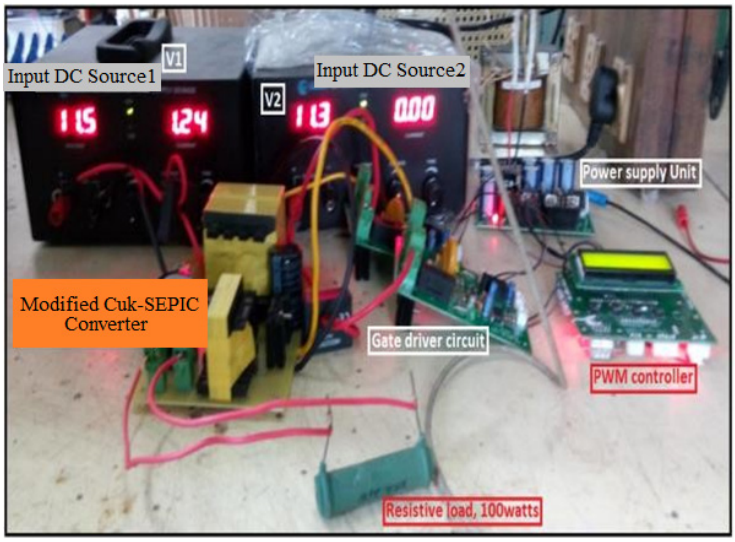

Figure 7. Prototype model of the modified Cuk-SEPIC converter

of 20 kHz. The MOSFET switches are triggered by the pulses generated by the controller. The duty cycle considered for the switch S1 is 50% and for S2 it is 25%. The gate pulses taken from the controller are shown in Figure 8 (a and b). The inductor voltages (VL1, VL2, VL3) and inductor L1 current and voltage are shown in Figure 8(c-f), respectively. The output voltage and output current are depicted in Figure 9 (a and b).

From the obtained results, it can be noted that the output voltage during the availability of both DC sources with the Field-Programmable Gate Array (FPGA) controller is 48.9V and the current is 8A.

From Table 4, it can be seen that the proposed Converter achieves the highest efficiency (95.77%) with a reduced number of components in comparison with the converter proposed by

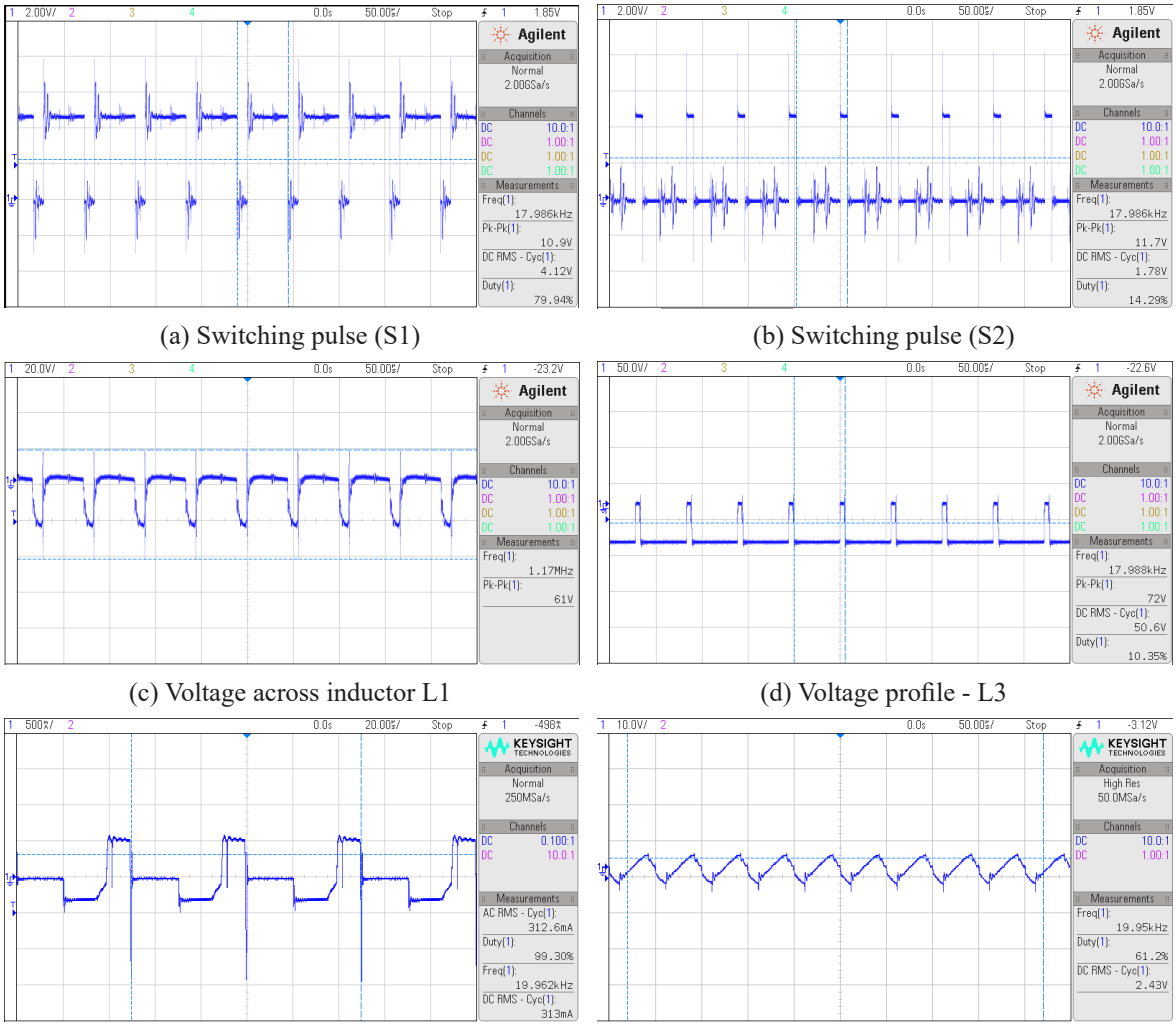

(a) Switching pulse (S1) (b) Switching pulse (S2)

(c) Voltage across inductor L1 (d) Voltage profile - L3

(e) Voltage profile – L2 (f) Inductor L1 current characteristic

Figure 8. Component Characteristics

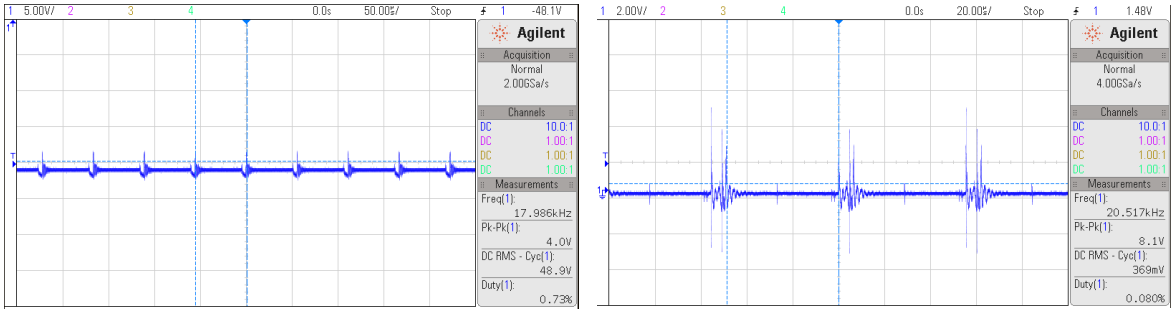

(a) Output voltage (b) Output current

Figure 9. Output Characteristics

Table 4. Comparison Analysis

Reference works	No. of Switches/Diodes	No. of Inductors/ Capacitors	Efficiency (%)
Natchimuthu, Chinnusamy & Mark (2020)	3/3	3/4	94.11
Jyothi et al. (2023)	1/3	3/3	91.4
Sathiya & Arun Noyal Doss (2023)	1/3	2/3	90.95
The proposed Converter	2/2	3/3	95.77

Natchimuthu, Chinnusamy & Mark (2020). When compared with the other three converters, it exhibits a significantly higher efficiency, which highlights its superior performance. Furthermore, it is evident that the power management system performs effectively under various combinations of input power sources to meet the load demand.

5. Conclusion

An optimized LQR control strategy for a modified Cuk-SEPIC dual-input DC-DC converter has been successfully developed and evaluated for hybrid photovoltaic-wind energy systems supplying remote telephony applications. The proposed converter topology ensures a continuous input current, an enhanced voltage gain, and an efficient power processing based on two renewable sources. The LQR controller, designed by using state-space modeling and a well-defined quadratic cost function, provides a superior dynamic performance by minimizing the voltage deviations and control effort. The simulation results confirm that the proposed controller provides a fast transient response, a reduced output voltage ripple, and robust stability under fluctuating input and load conditions. The overall system demonstrates a high reliability, which makes it a promising solution for off-grid telecommunication infrastructures where consistent and efficient power delivery is essential. Moreover, this control framework can be deployed for off-grid telecommunications, rural electrification, or microgrid applications. Thus, the simulation outcomes provide a strong foundation for a scalable, real-world hybrid PV-wind energy integration.

REFERENCES

Al-Ghussain, L., Ahmad, A.D., Abubaker, A.M. et al. (2023) Techno-economic feasibility of hybrid PV/wind/battery/thermal storage trigeneration system: Toward 100% energy independency and green hydrogen production. *Energy Reports*. 9, 752–772. https://doi.org/10.1016/j.egyr.2022.12.034.

Cholamuthu, P., Irusappan, B., Paramasivam, S.K. et al. (2022) A Grid-Connected Solar PV/Wind Turbine Based Hybrid Energy System Using ANFIS Controller for Hybrid Series Active Power Filter to Improve the Power Quality. *International Transactions on Electrical Energy Systems*. 2022(1), Art. ID 9374638. https://doi.org/10.1155/2022/9374638.

Duraisamy, M. (2024) Closed-loop Implementation of a Non-isolated High Step-up Integrated SEPIC-CUK DC-DC Converter Structure with Single Switch. *Brazilian Archives of Biology and Technology*. 67, Art. ID e24230787. https://doi.org/10.1590/1678-4324-2024230787.

Eltamaly, A.M., Alotaibi, M.A., Alolah, A.I. et al. (2021) IoT-Based Hybrid Renewable Energy System for Smart Campus. *Sustainability*. 13(15), Art. ID 8555. https://doi.org/10.3390/su13158555.

Icaza, D., Borge-Diez, D., Galindo, S.P. et al. (2020) Modeling and Simulation of a Hybrid System of Solar Panels and Wind Turbines for the Supply of Autonomous Electrical Energy to Organic Architectures. *Energies*. 13(18), Art. ID 4649. https://doi:10.3390/en13184649.

Jha, N., Prashar, D., Rashid, M. et al. (2022). Energy-Efficient Hybrid Power System Model Based on Solar and Wind Energy for Integrated Grids. *Mathematical Problems in Engineering*. 2022(1), Art. ID 4877422. https://doi.org/10.1155/2022/4877422.

Jyothi, B., Bhavana, P., Rao, B.T. et al. (2023) Implementation of Modified SEPIC Converter for Renewable Energy Built DC Microgrids. *International Journal of Photoenergy*. 2023(1), Art. ID 2620367. https://doi.org/10.1155/2023/2620367.

Katche, M.L., Makokha, A.B., Zachary, S. O. et al. (2023) A Comprehensive Review of Maximum Power Point Tracking (MPPT) Techniques Used in Solar PV Systems. *Energies*. 16(5), Art. ID 2206. https://doi.org/10.3390/en16052206.

Khan, M.U., Murtaza, A.F., Noman, A.M. et al. (2023) State-Space Modeling, Design, and Analysis

of the DC-DC Converters for PV Application: A Review. *Sustainability*. 16(1), Art. ID 202. https://doi.org/10.3390/su16010202.

Kushwaha, R., Singh, B. & Khadkikar, V. (2021) An Isolated Bridgeless Cuk-SEPIC Converter-Fed Electric Vehicle Charger. *IEEE Transactions on Industry Applications*. 58(2), 2512-2526. https://doi.org/10.1109/TIA.2021.3136496.

Mandal, S. & Prabhakaran, P. (2023) A Novel Bidirectional Modified SEPIC Converter with Wide Voltage Conversion Ratio. In: *2023 5th Biennial International Conference on Nascent Technologies in Engineering (ICNTE), 20-21 January 2023, Navi Mumbai, India*. New York, USA, IEEE. https://doi.org/10.1109/ICNTE56631.2023.10146642

Mamat, M.N. & Ishak, D. (2022) Analysis of SEPIC-Boost Converter Using Several PID Feedback Tuning Methods for Renewable Energy Applications. *Journal of Advanced Research in Applied Sciences and Engineering Technology*. 26(1), 105–117. https://doi.org/10.37934/araset.26.1.105117.

Mechnane, F., Drid, S., Nait-Said, N. et al. (2023) Robust Current Control of a Small-Scale Wind–Photovoltaic Hybrid System Based on the Multiport DC Converter. *Applied Sciences*. 13(12), Art. ID 7047. https://doi.org/10.3390/app13127047.

Natchimuthu, S., Chinnusamy, M. & Mark, A.P. (2020) Experimental investigation of PV based modified SEPIC converter fed hybrid electric vehicle (PV-HEV). *International Journal of Circuit Theory and Applications*. 48(6), 980–996. https://doi.org/10.1002/cta.2766.

Nirmala, R.G. & Venmathi, M. (2024) Investigations of DC-DC converter topologies for PV fed telecom applications. *AIP Conference Proceedings* (*International Conference on Advancement in Design, Development, Engineering, Processing, and Characterization: ADDEPC 2021, 1–2 December 2021, Virtual Conference*). 2853(1), Art. ID 020292. https://doi.org/10.1063/5.0197591.

Okilly, A.H. & Baek, J. (2021) Optimal Design Analysis with Simulation and Experimental Performance Investigation of High-Power Density Telecom PFC Converters. *Applied Sciences*. 11(17), Art. ID 7911. https://doi.org/10.3390/app11177911.

Paul, A.J., Kumar, C.A. & Carol, J.J. (2021) Investigation on extendable multiport DC–DC boost converter for hybrid renewable energy systems. *Automatika*. 62(3–4), 486–502. https://doi.org/10.1080/00051144.2021.1985704.

Ravada, B.R., Tummuru, N.R. & Ande, B.N.L. (2020) Photovoltaic-Wind and Hybrid Energy Storage Integrated Multi-Source Converter Configuration for DC Microgrid Applications. *IEEE Transactions on Sustainable Energy*. 12(1), 83–91. https://doi.org/10.1109/TSTE.2020.2983985.

Saha, P.K., Pal, N., Khan, F.A. et al. (2025) Modelling of small signals in MISO DC-DC converters for hybrid energy sources. *Microsystem Technologies*. 31, 1753–1761. https://doi.org/10.1007/s00542-024-05777-x.

Salimi, M., Radmand, F. & Firouz, M.H. (2021) Dynamic Modeling and Closed-loop Control of Hybrid Grid-connected Renewable Energy System with Multi-input Multi-output Controller. *Journal of Modern Power Systems and Clean Energy*. 9(1), 94-103. https://doi.org/10.35833/MPCE.2018.000353.

Sathiya, R. & Arun Noyal Doss, M. (2023) Design and implementation of single switch integrated boost and flyback converter for renewable and sustainable energy. *PLOS ONE*. 18(6), Art. ID e0287770. https://doi.org/10.1371/journal.pone.0287770.

Shen, Y., Chen, M., Majji, M. et al. (2023) Q-Markov Covariance Equivalent Realizations for Unstable and Marginally Stable Systems. *Mechanical Systems and Signal Processing*. 196, Art. ID 110343. https://doi.org/10.1016/j.ymssp.2023.110343.

Shunmathi, M. & Gnanavadivel, J. (2024) Modified Bridgeless PFC-Based Cuk-Sepic Converter With Improved Power Quality for Arc Welding Applications. *IETE Journal of Research*. 70(3), 3234-3244. https://doi.org/10.1080/03772063.2023.2190541.

Soldado-Guamán, J., Herrera-Perez, V., Pacheco-Cunduri, M. et al. (2023) Multiple input-single output DC-DC converters assessment for low power renewable sources integration. *Energies*. 16(4), Art. ID 1652. https://doi.org/10.3390/en16041652.

Ssenyimba, S., Kiggundu, N. & Banadda, N. (2020) Designing a solar and wind hybrid system for small-scale irrigation: a case study for Kalangala district in Uganda. *Energy, Sustainability and Society*. 10(1), Art. ID 6. https://doi:10.1186/s13705-020-0240-1.

Tenali, S., Ansari, A.A. & Praveen, J. (2021) Design of Cuk and Single-Ended Primary Inductor Converter (SEPIC) for PV Systems Integration to AC Grid. In: *2021 5th International Conference on Electronics, Communication and Aerospace Technology (ICECA)*, *2-4 December 2021*, Coimbatore, India. New York, USA, IEEE. pp. 44-47.

Vijayakumar, S. & Sudhakar, N. (2024) Golden eagle optimized fractional-order PI controller design for a PFC SEPIC converter in EV charging. *Scientific Reports*. 14(1), Art. ID 20954. https://doi.org/10.1038/s41598-024-69653-4.

Yao, X., Yi, B., Yu, Y., et al. (2020) Economic analysis of grid integration of variable solar and wind power with conventional power system. *Applied Energy*. 264, Art. ID 114706. https://doi.org/10.1016/j.apenergy.2020.114706.